In situ grown epitaxial heterojunction exhibits high-performance electrocatalytic water splitting

Zhu, Changrong; Wang, An-Liang; Xiao, Wen; Chao, Dongliang; Zhang, Xiao; Tiep, Nguyen Huy; Chen, Shi; Kang, Jiani; Wang, Xin; Ding, Jun; Wang, John; Zhang, Hua; Fan, Hong Jin

2018

Zhu, C., Wang, A.-L., Xiao, W., Chao, D., Zhang, X., Tiep, N. H., ⋯ Fan, H. J. (2018). In situ grown epitaxial heterojunction exhibits high-performance electrocatalytic water splitting. Advanced Materials, 30(13), 1705516-. doi:10.1002/adma.201705516

https://hdl.handle.net/10356/93043

https://doi.org/10.1002/adma.201705516

Advanced Materials

Epitaxial Nanoconfinement Enhanced Electro-catalyst for Water Splitting

--Manuscript Draft--

Manuscript Number:	
Full Title:	Epitaxial Nanoconfinement Enhanced Electro-catalyst for Water Splitting
Article Type:	Communication
Section/Category:	
Keywords:	Nanoconfinement; epitaxial in-growth; metal nitride nanoarrays; oxygen evolution reaction; hydrogen evolution reaction
Corresponding Author:	Hong Jin Fan Nanyang Technological University Singapore, SINGAPORE
Additional Information:	
Question	**Response**
Please submit a plain text version of your cover letter here. **If you are submitting a revision of your manuscript, please do not overwrite your original cover letter. There is an opportunity for you to provide your responses to the reviewers later; please do not add them here**.	Dear Editor, We are pleased to submit our new manuscript for publication consideration in Advanced Materials. In the energy community, people are developing non-precious metal electrocatalysts for HER/OER. It has been shown that multiple-element compounds and heterostructures generally show better performance than single oxides or carbides, because the interface electronic structure can be tailored. In this work, we present the epitaxial in-growth of Co@Ni3N nanoheterojunctions which are formed in-situ during nitridization of NiCo2O4 nanowires. The obtained Co@Ni3N nanoheterojunctions show outstanding electro-catalytic performance in both HER and OER. First-principle calculations show both interfacial epitaxy and interface electron transfer. Therefore, we ascribe the good electrocatalytic performance to a “nanoconfinement effect”, a phenomenon proposed and evidenced by Prof Bao Xinhe in other catalyst systems. In addition to electrocatalytic performance, we also show in details the enhanced capacitive energy storage of the Co-Ni3N nanowires due to increased overall electric conductivity. The highlights of our work: 1.Co-Ni3N nanoheterojucntions with epitaxial interface formed in situ. During the transformation from oxides to nitrides, epitaxial heterojunctions due to phase decomposition, leading to two materials with intimate-contact and stable interface. We show this structure functions better than single-phase metal oxides or nitrides. 2.One unique structure, multiple enhancements. The epitaxial in-grown Co-Ni3N nanoarrays inherit functions of both Co and Ni3N and also induces catalytic property enhancement due to interface charge transfer, and capacitive enhancement due to increased conductivity. For example, lowered switch on voltages for both HER and OER, and higher turn off frequency (TOF); and evidently improved rate performance as the supercapacitor electrode. Your consideration of this manuscript is highly appreciated. Sincerely, Hong Jin Fan School of Physical & Mathematical Sciences Nanyang Technological University Email: fanhj@ntu.edu.sg

Do you or any of your co-authors have a conflict of interest to declare?	No. The authors declare no conflict of interest.
Corresponding Author Secondary Information:	
Corresponding Author's Institution:	Nanyang Technological University
Corresponding Author's Secondary Institution:	
First Author:	Hong Jin Fan
First Author Secondary Information:	
Order of Authors:	Hong Jin Fan
	CHANGRONG ZHU
	Anliang Wang
Order of Authors Secondary Information:	
Abstract:	It is technologically important to develop non-precious metal electrocatalysts for water electrolysis and fuel cells. It is known that the electro-catalytic performance can be significantly enhanced by interface engineering a purposely-designed nanoheterojunction structure, where the interface electronic structure can be fine-tuned. Herein, we have devised a new approach of developing atomic epitaxial in-growth in Co-Ni3N nanowires array, where a nanoconfinement effect is reinforced at the interface. We attest by first-principle calculations that the nanoconfinement effect facilitates electron transfer at the epitaxial interface, leading to a significant enhancement in catalytic activities for both hydrogen and oxygen evolution reactions (10 and 16 times higher in the respective turn-over frequency compared to Ni3N-alone nanorods). This nanoconfinement effect occurring during in-situ atomic epitaxial in-growth of two compatible materials provides a new and more effective pathway than the commonly-studied ternary metal oxides or nitrides towards high-performance electrocatalysis.

Epitaxial Nanoconfinement Enhanced Electro-catalyst for Water Splitting

Changrong Zhu, An-liang Wang, Wen Xiao, Dongliang Chao, Xiao Zhang, Nguyen Huy Tiep, Shi Chen, Jiani Kang, Xin Wang, Jun Ding, John Wang, Hua Zhang*, Hong Jin Fan*

Dr. C. R. Zhu, Dr. D. L. Chao, Mr. Nguyen Huy Tiep, Dr. S. Chen, Prof. H. J. Fan*
School of Physical and Mathematical Sciences,
Nanyang Technological University, 637371, Singapore
* Email: fanhj@ntu.edu.sg

Dr. A.L. Wang, Dr. X. Zhang, Prof. H. Zhang*
Center for Programmable Materials, School of Materials Science and Engineering,
Nanyang Technological University, 639798, Singapore
* Email: HZhang@ntu.edu.sg

Mr. W. Xiao, Prof. J. Ding, Prof. J. Wang
Department of Material Science and Engineering,
National University of Singapore, 3 Engineering Drive, 117583, Singapore

Dr. C. R. Zhu, Prof. X. Wang
School of chemical and biomedical engineering
Nanyang Technological University, 637459, Singapore

Dr. C. R. Zhu, Dr. A. L. Wang and Mr. W. Xiao contributed equally to this work

Keywords: Nanoconfinement; epitaxial in-growth; metal nitride nanoarrays; oxygen evolution reaction; hydrogen evolution reaction

In recent years, tremendous efforts are being paid to sourcing high performance electrode materials for both energy storage [1-3] and energy conversion via electro-catalysts water-splitting.[4] For these applications, the electrode materials shall be of high electrical conductivity, superior electrochemical activity and reliable long-term durability, as well as low-cost. State-of-art high-efficiency electrode materials are, for example, RuO_2 for both supercapacitor and oxygen evolution reaction,[5] Pt for Hydrogen evolution[6] and oxygen reduction reaction.[7, 8] However, more attentions lie in low-cost non noble metal electrode materials, which are transition metal oxides,[9] sulfides,[10] phosphides,[11] carbides,[12] and nitrides.[13] The electrocatalyst performance of these compounds largely depend on the structure features at varying scales. Nevertheless, their performances are still far from satisfaction, and there is considerable room for improvement by, for example, elemental doping, [14-16] construction of core-shell structures[14, 17] and epitaxial growth,[6, 7, 18-20] in addition to discovery of new catalyst systems. Taking Ni_3N as an example, which is an intensively-studied electrocatalyst, Pt doping is shown to manifest capable of lowering the charge transfer resistance and thus improve the overall catalytic performance for HER.[21] In addition, a cheaper method of forming TiN@Ni_3N core-shell structure also presents a high catalytic current.[17] However, it also comes with a high overpotential, which is ascribed to the undesirable interface between TiN and Ni_3N, where a built-in electric field induces energy barrier for charge transfer. Among the attempts to enhance the electrocatalyst performance, an epitaxial growth with a lattice mismatch less than 5 % is preferable. [20] The epitaxial in-growth is generally advantageous in facilitating electron transfer between the two materials, and down-shifting the *d*-band center of metallic materials. However, conventional bottom-up epitaxial growths usually require a set of stringent processing conditions (as those in sputtering, thermal or e-beam lithography).[13, 27] In-situ epitaxal growth in a nanoscale without high temperature or vacuum may provide new opportunities.

The nano-confinement effect at the interface of two materials has been shown effective in reinforcing the co-existence of TiN and VN nanophases and the formation of Ti-V-N [22] epitaxial structure because of their lattice similarities. Inspired by this, we have sourced for the highly conductive candidates which share lattice similarities, and ideally can achieve synergy catalytic property. According to their crystal structures, Ni_3N and metallic Co have good lattice

matching (e.g., $d_{Ni3N\ (111)} \approx d_{Co\ (002)}$; $d_{Ni3N\ (002)} \approx d_{Co\ (100)}$ and $d_{Ni3N\ (302)} \approx d_{Co\ (103)}$. Ni_3N ref. JCPDS # 10-0280; Co ref. JCPDS # 89-4308). Thus, nanophased metallic Co and Ni_3N can be in-grown in an integrated nanostructure, and generate synergy in addition to inheriting their individual functions.

We herein report the development of Co@Ni_3N nanowires array with epitaxial in-grown internal structure, which are assembled on highly conductive carbon cloth. This nanowire arrays are thoroughly studied as electrocatalyst electrode for water splitting as well as supercapacitor. First-principle calculations not only supports the epitaxial interface but also implies efficient charge transfer across the Co@Ni_3N interface. In consequence, the nano-confinement effect drastically enhances electrochemical activity of the Co@Ni_3N epitaxial in-grown structure compared to the Ni_3N-alone nanorods electrodes; the TOF values for HER and OER of the Co-Ni_3N nanowires are 14.6 and 19.3 times larger than those of Ni_3N electrode, respectively. Our results by both experiment and calculation provide strong evidence to the advantage of confinement effect induced reinforcement in nanostructured electrocatalysts, which might be a generic effect in many similar metal@metal nitrides or sulfide systems.

Epitaxial in-growth and structure determination of Co-Ni_3N nanorods

The first-principles calculation suggests an epitaxial relationship between hexagonal cobalt metal (Co) and nickel nitride (Ni_3N), as illustrated in **Figure 1a**. The $(\bar{1}20)$ planes of hcp Co and Ni_3N in their unit cells are highlighted by the blue and pink planes respectively. The $(\bar{1}20)$ plane of Co is defined by two orthogonal vectors of Co [210] and Co [001] with 2.171 and 4.069 Å in length, respectively. Similarly, the $(\bar{1}20)$ plane of Ni_3N is defined by two orthogonal vectors of Ni_3N [210] and Ni_3N [001] with 4.005 and 4.306 Å in length, respectively. The length of Co [001] (4.069 Å) is close to that of Ni_3N [210] (4.005 Å) with only -1.56% in difference. Meanwhile, by doubling the length of Co [210] ($2 \times 2.171 = 4.342$ Å), Co [210] also matches well with that of Ni_3N [001] (4.306 Å) with a small variation of -0.83%. Therefore, an epitaxial relationship exists between the $(\bar{1}20)$ planes of hcp Co and Ni_3N by aligning Co [001] ([210]) with Ni_3N [210] ([001]) and straining Co [001] and [210] by -1.56% and -0.83% respectively. By comparing three different "sewing" modes, we have determined the most stable N-Co interface at the edge (**Figure S1**). The detailed interface is

illustrated in **Figure S2** (see detailed discussion in Mechanism study section).

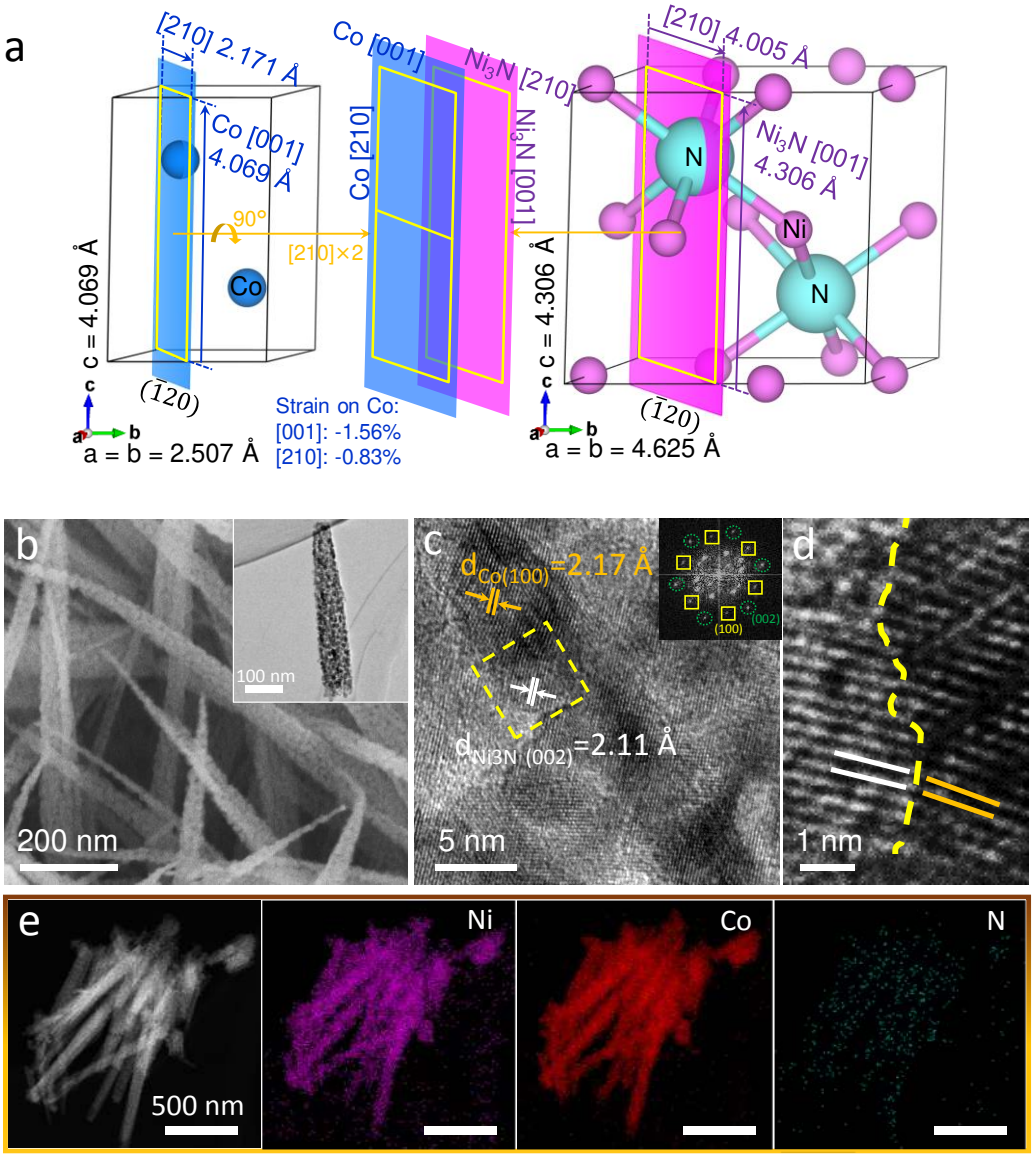

Figure 1. Formation of Co-Ni_3N nanorods with epitaxial in-growth structure. a) Schematic illustration of lattice matching of metallic Co and Ni_3N; SEM images of: b) the as-synthesized Co-Ni_3N nanorods (inset is the low magnification TEM image of a single Co-Ni_3N nanorod); c) and d) HRTEM images of Co-Ni_3N nanorods (inset in c is the corresponding FFT image from the dashed box area). The dashed box indicates the co-exist of Co (100) and Ni_3N (002) lattices, the dashed line indicates the interface between them; e) dark-field STEM image of Co-Ni_3N nanorods, and the corresponding STEM elemental mappings of Ni, Co and N.

To develop the epitaxial in-growth within the nanorods, we choose a source material that contains both Co and Ni which is $NiCo_2O_4$. The fabrication process for Co-Ni_3N nanorods

consists of two major steps, i.e. the hydrothermal growth of the source $NiCo_2O_4$ nanorods array, and the ammonia annealing at a proper temperature (Detailed synthesis conditions are given in experimental part in supporting information). As shown by the scanning electron microscope (SEM) images (**Figure 1b**), the as-synthesized Co-Ni_3N inherits the same morphology of the pristine $NiCo_2O_4$ nanorod (**Figure S3b**). Moreover, as confirmed by TEM studies (**Figure 1b** and S3d), the Co-Ni_3N nanoarrays (diameter ~ 80 nm, length ~ 1μm) are composed of tiny nanoparticles, which gives rise to a large surface area that are beneficial to improving electrochemical activity. Similarly, the Ni_3N nanophase (**Figure S4b**) maintains the morphology of its source NiO nanorod (**Figure S4a**). The lattices of both Ni_3N and Co are visible in the high resolution TEM (HRTEM) images (**Figure 1c**). The Fast Fourier Transition (FFT) images (inset in **Figure 1c)** also reveals the lattice planes of Ni_3N (002) and Co (100) pairs. Furthermore, there is clear demonstration for the coexistence of lattice fringes of metallic Co and Ni_3N, which are explicitly discerned in **Figure 1d** with clear interface. In addition, there is lattice transfer from Co (100) (perpendicular to Co (210)) to Ni_3N (002) (perpendicular to Ni_3N (210)), which are ascribed to the nanoconfinement effect that restricts these two sets of lattice in a single unit cell. The confinement with epitaxial interface prevents detachment of the two materials at the nanoscale, which is in accordance with the first-principle calculation results. Elemental mappings of Ni, Co and N correspond well to those profiles of Co-Ni_3N nanorods in **Figure 1e**.

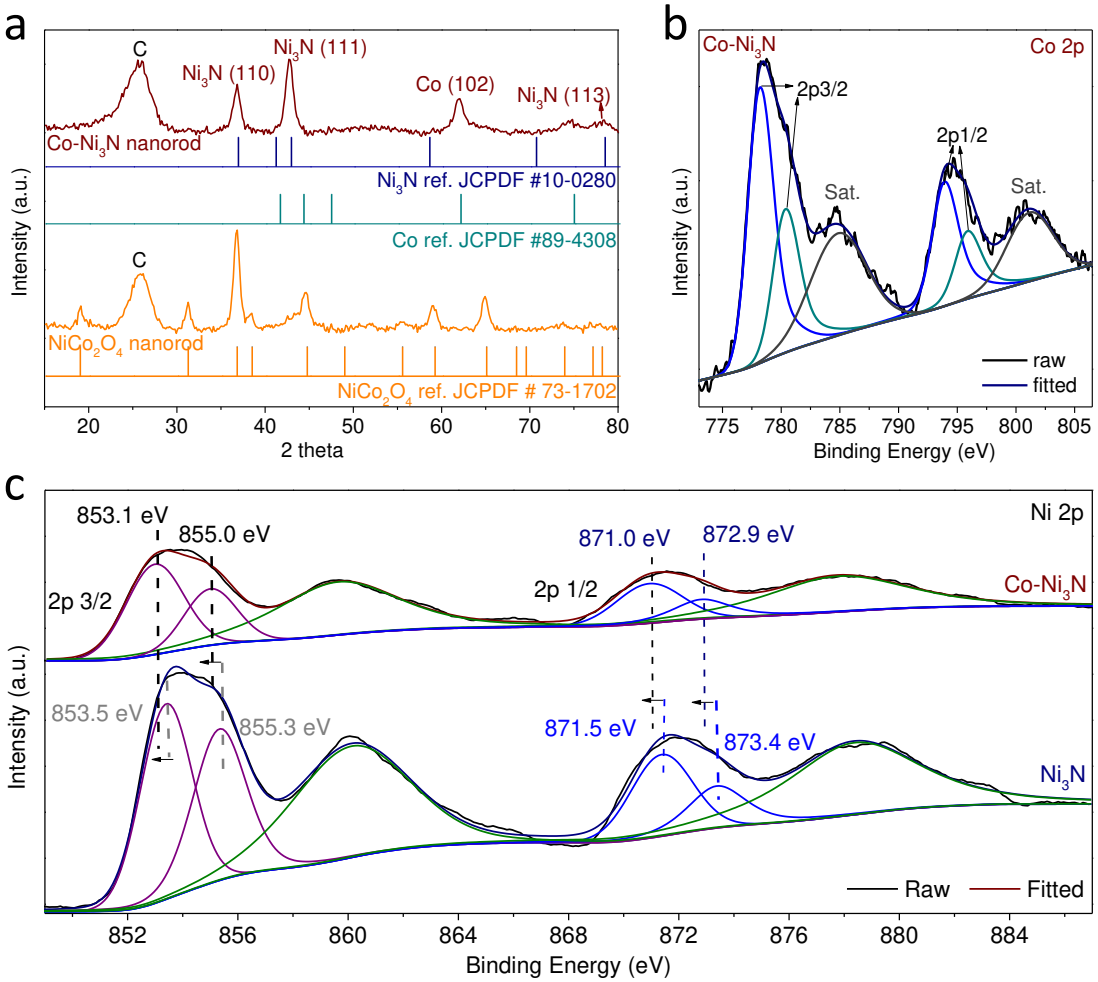

Figure 2. Structure characterization of Co-Ni_3N nanoarrays. a) XRD spectra of Co-Ni_3N and its source $NiCo_2O_4$ nanorods showing the complete transformation after ammonia annealing treatment; XPS spectrum of: b) Co 2p in Co-Ni_3N electrode, and c) Ni 2p signal comparison of Co-Ni_3N and Ni_3N electrode.

Further examination of the crystal structure of the Co-Ni_3N nanoarrays are made by the X-ray diffraction (XRD). As shown in **Figure 2a**, the XRD spectrum of Co-Ni_3N source material correspond well to the spinel $NiCo_2O_4$ structure (Joint Committee on Powder Diffraction Standards, JCPDS card no.73-1702). After thermal annealing in ammonia, the typical peaks of Ni_3N ((110) at $2\theta = 38.9^o$, (111) at $2\theta = 44.4^o$, (113) at $2\theta = 78.4^o$) and metallic Co ((102) at $2\theta = 62.4^o$, (110) at $2\theta = 75.9^o$) are observed, which are in agreement with JCPDS card no.10-0280 and 89-4308, respectively. In addition, X-ray photoelectron spectroscopy (XPS) was utilized to examine the sample surface. In the wide-scan range, sharp peaks of both N 1s and Ni 2p are detected in Co-Ni_3N and Ni_3N samples (**Figure S5b**). Analysis of XPS spectrum for Co 2p signal (**Figure 2b**) in Co-Ni_3N nanorods indicates that Co is mainly at zero valence state

(located at 778.1 and 781.1 eV) which is consistence with XRD and HRTEM studies. The other two peaks (794.3 and 797.3 eV) can be indexed to CoO, which may well be due to the slight oxidization of the sample when exposed to air before measurement.[23, 24] Meanwhile, two sharp peaks at around 853.1 and 871.0 eV (**Figure 2c**) belong to Ni 2p in Ni_3N, where Ni is prone to be at its low valence state similarly to that of Ni in the Ni_3N alone electrode.[25] The other two peaks at 855.0 and 872.9 eV may come from NiO resulted from partial oxidization of the Co-Ni_3N sample surface[14, 26, 27] It is noted that, for an identical peak, the binding energy of Ni 2p is slightly lower in Co-Ni_3N than that in Ni_3N, indicating extra charges in the Ni side, which need further confirmation by bader charge calculation. The binding energy of N 1s in Co-Ni_3N (**Figure S5c**) and Ni_3N (**Figure S5d**) is 398 and 398.7 eV, respectively, which are the typical peaks of the metal nitride. The slightly lower (~ 0.7 eV) binding energy of N 1s in Co-Ni_3N is also related to the charge accumulation in Ni_3N. The atomic concentration ratio of Ni to N is calculated to be 2.9:1, by integrating the peak areas with their sensitivity factors (N: 0.38; Ni: 5.4). Furthermore, the Raman shift peaks in Co-Ni_3N and Ni_3N are located in the similar position of ~ 460 cm^{-1} (**Figure S5a**), which is in accordance with the stretching mode of Ni-N bond.

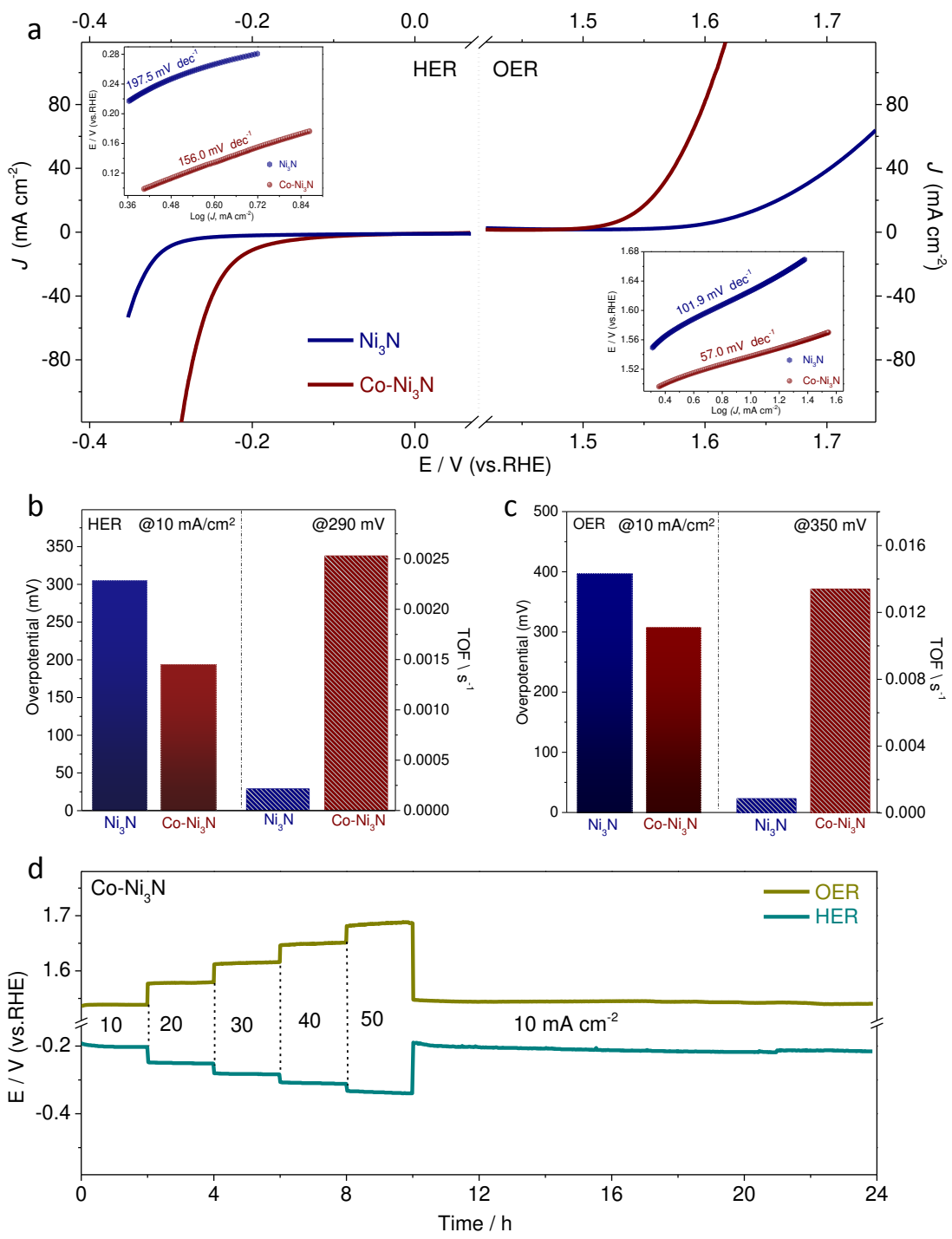

Figure 3. Electro-catalytic performance. a) LSV curves for the Co-Ni_3N and Ni_3N nanorod arrays for both hydrogen evolution reaction and oxygen evolution reaction catalyst (insets are the related Tafel plots for each application); b) Comparison of overpotentials of Ni_3N and Co-Ni_3N electrodes for HER at the current density of 10 mA cm^{-2} (left panel) and the corresponding TOF values at an overpotential of 290 mV (right panel). c) Comparison of overpotentials of Ni_3N and Co-Ni_3N electrodes for OER at the current density of 10 mA cm^{-2} (left panel) and the corresponding TOF values at an overpotential of 350 mV (right panel); d) stability tests of Co-Ni_3N at varied current densities for both HER and OER processes.

Electro-catalytic performance

In order to figure out the effect of nanoconfinement of Co-Ni_3N on catalytic performance, its electro-catalytic activity was investigated in N_2 saturated 1.0 M KOH solution using the typical three–electrode setup by liner sweep voltammetry (LSV) with Ni_3N as a comparison. Overall, the IR-corrected polarization curves for all samples (**Figure 3a**) clearly show that the Co-Ni_3N electrode owns better catalytic activity than that of Ni_3N for both hydrogen and oxygen evolution reaction (HER and OER). Specifically, for HER, the overpotential of Co-Ni_3N at 10 mA cm^{-2} (194 mV) is ~ 100 mV smaller than that of Ni_3N (305 mV). Meanwhile, at the overpotential of 290 mV, the current density of Co-Ni_3N is 14.6 times larger than that of Ni_3N (48.325 versus 3.318 mA cm^{-2}). The turnover frequency (TOF) value (**Figure 3b**) was calculated, based on the assumption that all metals in the catalysts were involved into the HER catalytic reaction. Clearly, Co-Ni_3N presents much higher turnover frequency with a TOF value of 0.1459 s^{-1} at the overpotential of 290 mV, which is 10 times of that for Ni_3N nanoarrays (0.0142 s^{-1}). The linear portions of Tafel plots were fit to Tafel equation ($\eta = a + b\log j$, where j is the current density and b is Tafel slope), yielding a Tafel slope of ~ 156.0 mV dec^{-1} for Co-Ni_3N (**Figure 3a**, upper left), which is lower than that of Ni_3N (197.5 mV dec^{-1}). The better conductivity of Co-Ni_3N nanoarrays, compared to that of Ni_3N, shall have contributed to the superior electro-catalytic performance. This is confirmed by the electrochemical impedance spectroscopy (EIS) study (**Figure 6b**), where Co-Ni_3N owns a low charge transfer resistance (~ 20 Ω), 10 times lower than that of Ni_3N electrode (~ 200 Ω).

For OER application, Co-Ni_3N needs 1.537 V (overpotential: 307 mV) to deliver a current density of 10 mA cm^{-2}, while Ni_3N requires a much larger overpotential of 1.627 V. The current density (127.87 versus 6.63 mA cm^{-2}) and TOF value of Co-Ni_3N (0.0134 s^{-1}) at the overpotential of 350 mV are 19.3 times and 15.8 times larger than that of Ni_3N (0.00086 s^{-1}), respectively. Moreover, the Tafel slope of Co-Ni_3N is 57.0 mV dec^{-1}, which is much smaller than that of Ni_3N (~ 101.9 mV dec^{-1}). Therefore, the Co-Ni_3N affords a larger current density and larger TOF value at lower overpotential, attributing to its unique epitaxial in-grown structure in the nanoarrays. In terms of the electrochemical conductivity, a smaller charge transfer resistance (2Ω) is observed for Co-Ni_3N than that of Ni_3N (9Ω) (**Figure S6d**), suggesting a much faster electron transfer during the electrochemical reaction, arising from the

existence of metallic Co nanophase in Co-Ni_3N.

To figure out the endurance of the electrodes towards repeating electro-catalytic processes, we applied a variety of current densities (10, 20, 30, 40 and 50 mA cm^{-2}) sequentially for 10 h on the Co-Ni_3N electrode both for HER and OER (**Figure 3d**). In overall, the overpotential to deliver certain current density remains almost unchangeable, which indicates the excellent stability of Co-Ni_3N, due to the high integrity of the nanostructure. In particular, when the current density is reverted to 10 mA cm^{-2} after undergoing high current density flow, the voltage rapidly resumes and prevails over an additional prolonged 20 h test. The overpotential values for both HER and OER are mostly recovered, when switched back to 10 mA cm^{-2}. This demonstrates the stability and durability of the Co-Ni_3N nanostructure, capable of sustaining high current flow and fast electron movement. Furthermore, when extend the test to 20 hours, the Co-Ni_3N nanoarrays remains a better durability with a lower stable overpotential than that of Ni_3N electrode both for HER (**Figure S6a**) and OER (**Figure S6c**). It should be noted that, while our XPS study of the electrode after the OER test did not indicate oxidation of Ni_3N, the possibility of slight surface oxidation should not be ruled out, which has been commonly observed in a few nanostructured metal nitride based OER electrode.

Mechanism Study

Comprehensive first-principles calculations are performed to investigate the stability and charge transfer at the Co/Ni_3N $(\bar{1}20)$ interface. First of all, different Co/Ni_3N $(\bar{1}20)$ interface structures, including N-Co-interface, Ni1-Co-interface and Ni2-Co-interface (see **Figure S1** and **S2**), are constructed, and attempted by aligning Co [001] ([210]) with Ni_3N [210] ([001]) and straining Co [001] and [210] by -1.56% and -0.83%, respectively. Therein, the N-Co-interface is found to be the most stable due to a small interfacial energy of -181~-178 meV/$Å^2$ (**Figure S1**). The negative value means that the N-Co-interface will readily form when combining hcp Co and Ni_3N during synthesis. This is possible because the N-terminated plane of Ni_3N and Co-terminated plane of Co form stable N-Co bonds as in CoN. Furthermore, the b-c plane of the N-Co-interface model in **Figure 1a** left and **Figure 1b** up can be indexed to the Co (100) plane and Ni_3N (002) plane, which are also observed in the TEM observation. It suggests that the *N-Co-interface model* supports our experimental observation.

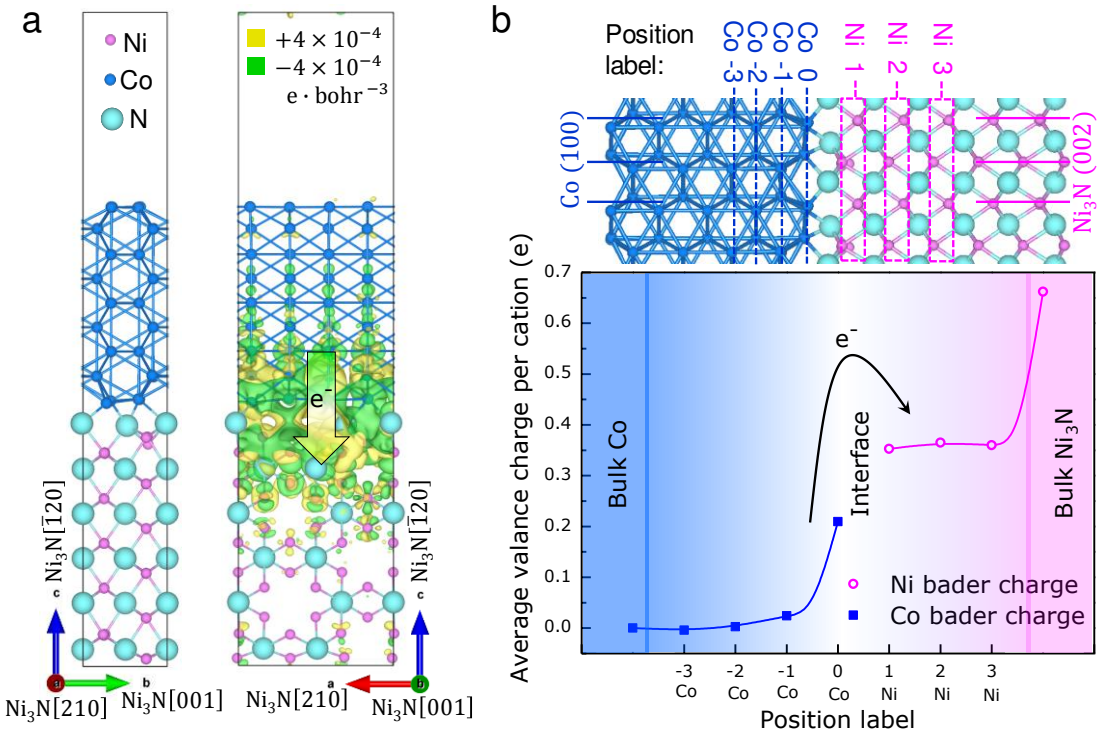

Figure 4. First-Principles calculations to illustrate interface charge transfer. a) Structures of the N-Co-interface formed between hcp Co and Ni_3N by joining N-terminated $(\bar{1}20)$ slab of Ni_3N and Co-terminated $(\bar{1}20)$ slab of hcp Co. Charge density difference due to the formation of interface is displayed on the right, where the yellow and cyan represent electron accumulation ($\Delta\rho = +6 \times 10^{-4}\ e \cdot \text{bohr}^{-3}$) and depletion ($\Delta\rho = -6 \times 10^{-4}\ e \cdot \text{bohr}^{-3}$), respectively; b) Bader charge analysis of Co and Ni cations near the N-Co-interface and in bulk Co and Ni_3N, respectively.

Interface charge transfer enhances the electro-catalytic activity for HER. The charge density difference in **Figure 4a** right illustrates that electrons transfer from Co to Ni_3N, where Ni and Co cations near the interface gain and loss electrons respectively. Moreover, bader charge analysis is performed on the Ni and Co cations at the N-Co interface and bulk models, as seen in **Figure 4b**. The average valence charge of Co increases with decreasing distance to the interface. On the contrary, the average valence charge of Ni decreases with decreasing distance to the interface. It affirms that electrons transfer from the Co to Ni cations near the interface, which can be due to the interfacial Co 3d-N 2p-Ni 3d hybridizations (**Figure S8**). It has been reported that the active HER site in Ni_3N is on Ni cations with a positive free energy change.[21,

[28-31] Therefore, the rate limiting step for the HER process is the unstable absorption of H adatom on Ni. [32] By transferring electrons from Co to Ni near the N-Co-interface,[40] [33] the additional electrons on Ni will stabilize the H adatom and hence benefit the HER catalytic activity.[34-37]

It is reported that the active HER site in Ni_3N is on 3-fold Ni hollow site having a positive free energy change G_{H^*}. [32] The positive G_{H^*} reveals that the rate limiting step for HER process on Ni_3N is the unstable adsorption of H adatom. **Figure S9** shows the calculated HER free energy diagrams for various Ni hollows sites near the N-Co-interface. The G_{H^*} decreases from ~0.10 eV (position 3) to ~0.04 eV (position 1) with decreasing distance between the HER site and the N-Co-interface. It shows that the Ni hollow site close to the interface has superior HER activity compared to those farther away from the interface. This is in consistent with our interface charge transfer argument; Electrons transfer from Co to Ni near the N-Co-interface and the additional electrons on Ni can stabilize the H adatom giving rise to a much reduced G_{H^*}. Therefore, our first-principles calculations unveil that the epitaxial interface between Ni_3N and Co enhances the HER activity of Ni_3N by inducing electron transfer from Co to Ni.

Furthermore, nanostructured metal nitrides are also commonly investigated for supercapacitor applications, in which reversible surface redox reactions give rise to fast charge storage/release performance. We also employed the Co-Ni_3N nanorods as pseudocapacitive cathode and compared to the pure Ni_3N (see **Figure S10 and S11** for detailed characterization and related discussion in Supporting Information). It is found that, compared to the pure Ni_3N nanorods electrode, the Co-Ni_3N nanorods array has a more capacitive behavior and better tolerance to high scan speeds. This difference can also be attributed to the better conductivity and electrochemical stability of the Co-Ni_3N nanorods, in consistence with the above result. Interestingly, the quasi-rectangular CV loops with absence of evident redox peaks may imply that the Co or Ni_3N are not seriously oxidized (despite unavoidable surface partial oxidation) during the measurements.

To wrap up, in connection with discussions above, four points are worth highlighting of the Co-Ni_3N nanoarrays electrode synthesized in the present study: *firstly*, the combination of the two structurally matching materials of Co and Ni_3N with similar lattice parameters can inherit the characteristics of both nanophases, i.e., Co-Ni_3N combines the high activity for Herovsky

and Tafel steps and can quickly desorb the OH^- during the reactions. *Secondly*, the introduction of the metallic Co nanophase efficiently enhances the overall electrical conductivity, which is key to both the fast charge transports in the HER/OER processes and the capacitive process in pseudocapacitive charge storage. *Thirdly*, the epitaxial in-grown interface between Co and Ni_3N facilitates electron transfer between the two phases (from Co to Ni), which will stabilize the H adatom and lower the HER free energy thus benefiting the HER catalytic activity. *Finally*, the nanorod structure not only increases the surface areas compared to films, but also facilitate quasi-one-dimensional charge transport along the nanorods, leading to excellent electrochemical activity.

In conclusion, we have developed a well-configured nanoarrays structure for Co-Ni_3N, derived from the corresponding oxide precursor, where epitaxial in-growth of the two structurally matching nanophase takes place, giving rise to unique nanoconfinement at the interface. The Co-Ni_3N nanoarrays thus-derived inherit the functions of both Co and Ni_3N, together with the refined structural features and epitaxial interface, leading to high performance for hydrogen and oxygen evolution reactions, with a lower switch on potential, faster turn over speed and better long-term durability being observed. Furthermore, when employed as a supercapacitor cathode, the Co-Ni_3N nanoarrays demonstrate the dominating capacitive process, giving rise to high-rate charge storage performance. This work demonstrates a new pathway for developing nanostructured electrode materials, where the two structurally matching nanophases are synergized by an epitaxial in-grown interface leading to much enhanced electrocatalytic performance.

Acknowledgements

H. J. Fan acknowledges the financial supported by MOE AcRF Tier 1 (RG117/16) and Tier 2 (MOE2017-T2-1-073). H.Z. thanks the support from MOE under AcRF Tier 2 (ARC 19/15, No. MOE2014-T2-2-093; MOE2015-T2-2-057; MOE2016-T2-2-103) and AcRF Tier 1 (2016-T1-001-147; 2016-T1-002-051), and NTU under Start-Up Grant (M4081296.070.500000) in Singapore. J. Ding and J. Wang thank the support from NRF-CRP16-2015-01.

Reference

[1] M.-S. Balogun, Y. Huang, W. Qiu, H. Yang, H. Ji, Y. Tong, *Mater. Today* **2017**.
[2] N. Choudhary, C. Li, J. Moore, N. Nagaiah, L. Zhai, Y. Jung, J. Thomas, *Adv. Mater.* **2017**, 1605336.
[3] G. Wang, L. Zhang, J. Zhang, *Chem Soc Rev* **2012**, *41*, 797.
[4] S. J. C. Robinson, D. M. Heinekey, *Chem. Commun.* **2017**.
[5] J. Xu, Q. Wang, X. Wang, Q. Xiang, B. Liang, D. Chen, G. Shen, *ACS Nano* **2013**, *7*, 5453.
[6] T. Bian, H. Zhang, Y. Jiang, C. Jin, J. Wu, H. Yang, D. Yang, *Nano Lett.* **2015**, *15*, 7808.
[7] C. Meng, T. Ling, T.-Y. Ma, H. Wang, Z. Hu, Y. Zhou, J. Mao, X.-W. Du, M. Jaroniec, S.-Z. Qiao, *Adv. Mater.* **2017**, *29*, 1604607.
[8] J. Li, H.-M. Yin, X.-B. Li, E. Okunishi, Y.-L. Shen, J. He, Z.-K. Tang, W.-X. Wang, E. Yücelen, C. Li, Y. Gong, L. Gu, S. Miao, L.-M. Liu, J. Luo, Y. Ding, **2017**, *2*, 17111.
[9] H. Jiang, J. Ma, C. Li, *Adv. Mater.* **2012**, *24*, 4197.
[10] Q. Lu, Y. Yu, Q. Ma, B. Chen, H. Zhang, *Adv. Mater.* **2016**, *28*, 1917.
[11] Y. Shi, B. Zhang, *Chem. Soc. Rev.* **2016**, *45*, 1529.
[12] Y. Zhong, X. Xia, F. Shi, J. Zhan, J. Tu, H. J. Fan, *Advanced Science* **2016**, *3*.
[13] S. Dong, X. Chen, X. Zhang, G. Cui, *Coord. Chem. Rev.* **2013**, *257*, 1946.
[14] B. Zhang, C. Xiao, S. Xie, J. Liang, X. Chen, Y. Tang, *Chem. Mater* **2016**, *28*, 6934.
[15] M. Chen, Y.-J. Zhao, J.-H. Liao, X.-B. Yang, *Phys. Rev. B* **2012**, *86*, 045459.
[16] J. Luo, Z.-J. Cui, G.-L. Zang, *Journal of Chemistry* **2013**, *2013*.
[17] Q. Zhang, Y. Wang, Y. Wang, A. M. Al-Enizi, A. A. Elzatahry, G. Zheng, *J. Mater. Chem. A* **2016**, *4*, 5713.
[18] C. Hahn, T. Hatsukade, Y.-G. Kim, A. Vailionis, J. H. Baricuatro, D. C. Higgins, S. A. Nitopi, M. P. Soriaga, T. F. Jaramillo, *Proc. Natl. Acad. Sci.* **2017**, *114*, 5918.
[19] W. Wang, J. Goebl, L. He, S. Aloni, Y. Hu, L. Zhen, Y. Yin, *J. Am. Chem. Soc.* **2010**, *132*, 17316.
[20] X. Huang, Z. Zeng, S. Bao, M. Wang, X. Qi, Z. Fan, H. Zhang, *Nat. Commun.* **2013**, *4*, 1444.
[21] Y. Wang, L. Chen, X. Yu, Y. Wang, G. Zheng, *Adv. Energy Mater.* **2017**, *7*, 1601390.
[22] A. Fischer, J. O. Müller, M. Antonietti, A. Thomas, *ACS Nano* **2008**, *2*, 2489.
[23] M. Yu, Z. Wang, C. Hou, Z. Wang, C. Liang, C. Zhao, Y. Tong, X. Lu, S. Yang, *Adv. Mater.* **2017**, 1602868.
[24] H. Liang, A. N. Gandi, D. H. Anjum, X. Wang, U. Schwingenschlögl, H. N. Alshareef, *Nano Lett.* **2016**, *16*, 7718.
[25] C. Liu, C. Li, K. Ahmed, Z. Mutlu, C. S. Ozkan, M. Ozkan, *Scientific Reports* **2016**, *6*.
[26] J. Li, M. Yan, X. Zhou, Z. Q. Huang, Z. Xia, C. R. Chang, Y. Ma, Y. Qu, *Adv. Funct. Mater.* **2016**, *26*, 6785.
[27] M. Görlin, J. Ferreira de Araújo, H. Schmies, D. Bernsmeier, S. Dresp, M. Gliech, Z. Jusys, P. Chernev, R. Kraehnert, H. Dau, P. Strasser, *J. Am. Chem. Soc.* **2017**, *139*, 2070.
[28] Y. Yu, W. Gao, Z. Shen, Q. Zheng, H. Wu, X. Wang, W. Song, K. Ding, *J. Mater. Chem. A* **2015**, *3*, 16633.
[29] M. Zeng, Y. Li, *J. Mater. Chem. A* **2015**, *3*, 14942.
[30] Y. Zheng, Y. Jiao, M. Jaroniec, S. Z. Qiao, *Angew. Chem. Int. Ed.* **2015**, *54*, 52.
[31] X. Wang, X. Gan, T. Hu, K. Fujisawa, Y. Lei, Z. Lin, B. Xu, Z. H. Huang, F. Kang, M. Terrones, R. Lv, *Adv Mater* **2017**, *29*.
[32] D. Gao, J. Zhang, T. Wang, W. Xiao, K. Tao, D. Xue, J. Ding, *J. Mater. Chem. A* **2016**, *4*, 17363.
[33] M. D. Meganathan, S. Mao, T. Huang, G. Sun, *J. Mater. Chem. A* **2017**.
[34] Y. Surendranath, M. W. Kanan, D. G. Nocera, *J. Am. Chem. Soc.* **2010**, *132*, 16501.
[35] A. E. Mattsson, P. A. Schultz, M. P. Desjarlais, T. R. Mattsson, K. Leung, *Modell. Simul. Mater. Sci. Eng.* **2005**, *13*, R1.
[36] X. Huang, M. Leng, W. Xiao, M. Li, J. Ding, T. L. Tan, W. S. V. Lee, J. Xue, *Adv. Funct. Mater.* **2017**, *27*.
[37] Z. W. Seh, J. Kibsgaard, C. F. Dickens, I. Chorkendorff, J. K. Norskov, T. F. Jaramillo, *Science* **2017**, *355*.